

Neural network analysis for prediction of heat transfer of aqueous hybrid nanofluid flow in a variable porous space with varying film thickness over a stretched surface

Abeer S Alnahdi and Taza Gul

Citation : Chin. Phys. B, 2025, 34 (**2**): 024701. DOI: 10.1088/1674-1056/ad989c
Journal homepage: http://cpb.iphy.ac.cn; http://iopscience.iop.org/cpb

What follows is a list of articles you may be interested in

Casson hybrid nanofluid flow over a Riga plate for drug delivery applications with double diffusion

Abeer S. Alnahdi and Taza Gul
Chin. Phys. B, 2024, 33 (**10**): 104701. DOI: 10.1088/1674-1056/ad624e

Influence of various shapes of nanoparticles on unsteady stagnation-point flow of Cu-H_2O nanofluid on a flat surface in a porous medium: A stability analysis

Astick Banerjee, Krishnendu Bhattacharyya, Sanat Kumar Mahato, and Ali J. Chamkha
Chin. Phys. B, 2022, 31 (**4**): 044701. DOI: 10.1088/1674-1056/ac229b

Induced magnetic field stagnation point flow of nanofluid past convectively heated stretching sheet with Buoyancy effects

Tanzila Hayat, S Nadeem
Chin. Phys. B, 2016, 25 (**11**): 114701. DOI: 10.1088/1674-1056/25/11/114701

Three-dimensional magnetohydrodynamics axisymmetric stagnation flow and heat transfer due to an axisymmetric shrinking/stretching sheet with viscous dissipation and heat source/sink

Dinesh Rajotia, R. N. Jat
Chin. Phys. B, 2014, 23 (**7**): 074701. DOI: 10.1088/1674-1056/23/7/074701

Variable fluid properties and variable heat flux effects on the flow and heat transfer in a non-Newtonian Maxwell fluid over an unsteady stretching sheet with slip velocity

Ahmed M. Megahed
Chin. Phys. B, 2013, 22 (**9**): 094701. DOI: 10.1088/1674-1056/22/9/094701

Neural network analysis for prediction of heat transfer of aqueous hybrid nanofluid flow in a variable porous space with varying film thickness over a stretched surface

Abeer S Alnahdi[1,†] and Taza Gul[2,3]

[1] *Department of Mathematics and Statistics, Faculty of Science, Imam Mohammad Ibn Saud Islamic University (IMSIU), Riyadh, Saudi Arabia*
[2] *Mathematics Department, City University of Science and Information Technology, Peshawar, 25000, Pakistan*
[3] *DoST-Directorate General of Science and Technology Khyber Pakhtunkhwa, Peshawar, 25000, Pakistan*

(Received 29 July 2024; revised manuscript received 27 September 2024; accepted manuscript online 29 November 2024)

The high thermal conductivity of the nanoparticles in hybrid nanofluids results in enhanced thermal conductivity associated with their base fluids. Enhanced heat transfer is a result of this high thermal conductivity, which has significant applications in heat exchangers and engineering devices. To optimize heat transfer, a liquid film of Cu and TiO_2 hybrid nanofluid behind a stretching sheet in a variable porous medium is being considered due to its importance. The nature of the fluid is considered time-dependent and the thickness of the liquid film is measured variable adjustable with the variable porous space and favorable for the uniform flow of the liquid film. The solution of the problem is acquired using the homotopy analysis method HAM, and the artificial neural network ANN is applied to obtain detailed information in the form of error estimation and validations using the fitting curve analysis. HAM data is utilized to train the ANN in this study, which uses Cu and TiO_2 hybrid nanofluids in a variable porous space for unsteady thin film flow, and it is used to train the ANN. The results indicate that Cu and TiO_2 play a greater role in boosting the rate.

Keywords: thin film of Cu and TiO_2 hybrid nanofluids, variable porous space, unsteady stretching sheet, viscous dissipation, heat transfer optimization, artificial neural network

PACS: 47.15.gm, 47.15.Cb, 44.20.+b, 44.05.+e

DOI: 10.1088/1674-1056/ad989c **CSTR:** 32038.14.CPB.ad989c

1. Introduction

Thin film or liquid film flow is a thin tinny layer of liquid used as a coating, lubricant, adhesive, and paint, on the surfaces of sheets to work in manufacturing and printing. Thin film flow is a result of the fluid layer being very thin and is connected to the dimensions of the surface through which it flows. Compared to liquid flow of ingredients, this consequence involves different flow actions that involve surface tension, capillary forces, and possibly instability caused by gravity or other external forces.

The use of thin film in extraction and absorption can enhance mass transfer. Different components can be efficiently contacted and separated thanks to the thin liquid film. Thin film flow is also operated in heat exchangers to increase heat transfer (HT) between a hot and cold fluid as shown in Neeraas *et al.*[1] They claimed that effective heat transfer (HT) is facilitated by the thin liquid film's function as a thermal boundary layer. In several coating and deposition procedures, including spray coating, spin coating, and dip coating, liquid film flow is essential. The homogeneous and even coating thickness on the substrate established by Weinstein *et al.*[2] is ensured by the regulated flow of liquid film. In the field of thin film technology, liquid film flow has been thoroughly explored for applications such as solar cells, optical coatings, and microelectronics. To achieve the necessary thin film qualities, it is imperative to comprehend and regulate the behavior of liquid film flow.

Ibrahim *et al.*[3,4] clarified fluid film stream is utilized in wastewater treatment forms, Such as streaming channels and biofilm reactors. The thin fluid film gives a huge surface range for the connection and development of microorganisms, supporting the degradation of natural matter. Vo *et al.*[5] examined fluid film flow in surface science to examine the wetting behavior of fluids on diverse surfaces. It is additionally critical in tribology, the think about contact, wear, and grease, as the nearness of fluid movies can impact contact and wear characteristics.

Craster and Matar[6] considered thin film flow over a stretched surface and observed that it is an essential problem in the field of engineering[7,8] have investigated the flow of thin films over an unsteady stretched surface. The small particles (NPs) in nanometer size consist of metals, carbides, and oxides that are dispersed in the base fluid to perform nanofluids (NFs). The NFs exhibit improved thermal prop-

†Corresponding author. E-mail: asalnahdi@imamu.edu.sa

© 2025 Chinese Physical Society and IOP Publishing Ltd. All rights, including for text and data mining, AI training, and similar technologies, are reserved.

erties compared to the base fluid.[9,10] The NFs have limited thermophysical and chemical properties. Therefore to fill this gap the researchers introduced an advanced class of nanofluids which is the combination of two different materials with different characteristics and dispersible in a single base fluid. This class is known as the hybrid nanofluids (HNFs). Cu and TiO_2 HNFs are a type of nanofluids that consists of a combination of copper (Cu) NPs and titanium dioxide (TiO_2) NPs suspended in a base fluid. The addition of Cu NPs to the TiO_2 nanofluids improves their thermal conductivity (TC) due to the high TC of copper. This enhanced TC allows for efficient heat transfer (HT) within the nanofluid (NF), making it a promising coolant in heat exchangers and thermal management systems.[11] Jana *et al.*[12] described the addition of NPs with high TC improves the thermal efficiency of the fluid, and makes it beneficial for cooling purposes in electronic devices, and heat exchangers[13–16] have focused on the HNFs to study their uses in medicine, and drug delivery. Khodadadi *et al.*[17] have studied the HNFs in the context of an industrial perspective using their rheological properties. These properties are usually used in the form of polymeric melts, fibers, and extrusions. Waseem *et al.*,[18] Ramzan *et al.*[19] examined the HNFs in terms that HNFs possess catalytic NPs that function in catalysis, increasing reaction rates, and whole efficiency. The use of HNFs in progressive freezing systems, such as automotive heaters, is extensive and mainly focused on their higher thermal conductivity (TC). The HNFs are also used to enhance the oil recovery (EOR) from the oil reservoir in terms of the mechanical agents as stated in Sun *et al.*[20]

The electrical conductivity of the HNFs is used by Xian *et al.*[21] in microdevices to stabilize the heat dissipation. The stretching surface's fluid flow has significant applications in industry and heat exchangers. The paints, corrosion, and polymer industries frequently use these types of studies.[22] Andersson *et al.*[23] connected the heat and mass transfer phenomena in the fluid flow with the industry. This phenomenon includes polymer stretching, extrusion, spinning of fiber, and wire coating. The applications regarding thin-film flow in the field of fluid dynamics include film production, lubrications, paints, wrapping, and electronics.[24] Similarly, it works as medication and importantly works in the uniformity of blood flow by sustaining the stability in its viscosity.[25,26] The porous space has also an important role in heat transfer using HNFs. The porous space reduces the flow dynamics by keeping the fluid for some time and consequently increases the fluid temperature. Where the variable characteristics of the porous space are more suitable for the stabilization of the fluid flow for the desired thermal applications.

In the case of the thin film the variable porous space, expressively increases the HT rate in thin film flows of HNFs. The variable porous space provides a larger surface area, which allows sufficient surface area for the flow of hybrid nanofluids (HNFs) and consequently enhances the heat transfer (TC) ability.[27]

The important feature of the variable porous space is to control the flow behavior of thin films of HNFs. The adjustment of pore size depends on the variable porosity concept, which allows the uniform distribution of the thin film.[28,29] Based on the above literature and discussion the current analysis is extended using the novelty and importance of the current work.

Newness of the present work is listed below.

(i) In thin film flows of HNFs, particle deposition happens on the surface of the solid. The variable porous space helps in adjusting particle deposition by letting the deposition arise within the pores despite the solid surface. Therefore, the porous space is considered variable for the first time for the thin film flow of HNFs over a stretching surface.

(ii) Liquid film of Cu and TiO_2 hybrid nanofluid (HNF) is considered for the enhancement of heat transfer (HT) and the variable porous space plays a role in improving the thermal efficiency of the HNFs.

(iii) The HAM solution is tackled by artificial neural network (ANN) and this is the advanced technique to solve the proposed model.

The physical sketch of our model is shown in Fig. 1.

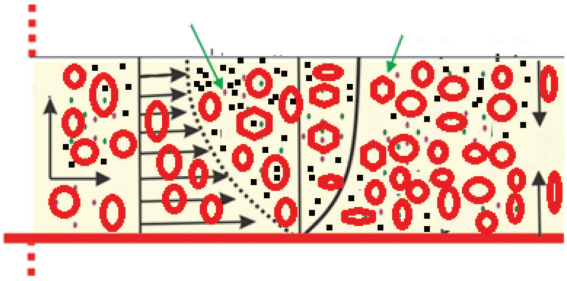


Fig. 1. The physical sketch of the present study.

2. Formulation

The study considered investigating the impact of the thin film flow of Cu and TiO_2 hybrid nanofluids over an extending surface in a variable porous space. The copper (Cu) and titanium dioxide (TiO_2) nanomaterials are dispersed in a base fluid of water to perform a hybrid nanofluid (HNF). The flow scenario of the thin film of HNFs includes analyzing the velocity profiles, temperature profiles, and heat transfer (HT) characteristics. The fluid flow is considered incompressible, and unsteady thin film Cu and TiO_2 HNFs. The flow is also considered laminar, such that the fluid particles do not collide in such

a manner to produce turbulence. In the current model, the surface is continually extending in x direction, affecting the fluid to pull along with it. The sheet is stretched with an unsteady velocity $U_{\rm w} = bx(1-\gamma t)^{-1}$, where γ is the unsteady rate and b is the stretching rate. The temperature of the stretched surface is assumed

$$T_{\rm w}(x,t) = T_0 - T_{\rm r}\left[bx^2(2\upsilon)^{-1}\right](1-\gamma t)^{-3/2},$$

where T_0 and $T_{\rm r}$ are the initial and reference temperature components such that $0 < T_{\rm r} < T_0$. The existing literature[7,8,28,29,39,40] has defined the following basic governing equations:

$$\frac{\partial u}{\partial x} + \frac{\partial v}{\partial y} = 0, \tag{1}$$

$$\rho_{\rm hnf}\left[\frac{\partial u}{\partial t} + u\frac{\partial u}{\partial x} + v\frac{\partial u}{\partial y}\right] = \frac{\partial}{\partial y}\left(\mu_{\rm hnf}\frac{\partial u}{\partial y}\right) - \frac{\upsilon_{\rm nf}}{K(x)}u, \tag{2}$$

$$(\rho C_p)_{\rm hnf}\left[\frac{\partial T}{\partial t} + u\frac{\partial T}{\partial x} + v\frac{\partial T}{\partial y}\right] = k_{\rm hnf}\frac{\partial^2 T}{\partial y^2} + \mu_{\rm hnf}\left(\frac{\partial u}{\partial y}\right)^2, \tag{3}$$

where $\rho_{\rm hnf}$ is the density of the HNFs, $h(t)$ is the film thickness, t is time, u, v are the velocity field components, $\mu_{\rm hnf}$ is the dynamic viscosity of HNFs, and $K(x)$ is the permeability term function of x that vary along the x-axis in the porous medium.

The initial and boundary conditions for the thin film HNFs flow are[7,8]

$$\begin{aligned} &u = u_{\rm w}, \quad v = 0, \quad \text{at} \quad y = 0,\\ &\frac{\partial u}{\partial y} = 0, \quad \frac{\partial T}{\partial y} = 0, \quad \text{and} \quad v = \frac{\partial h}{\partial t} \ \text{at}\ y = h(t). \end{aligned} \tag{4}$$

Here $u = u_{\rm w}$ shows the stretching velocity of the sheet along the x-axis. The term $\partial u/\partial y$ shows the velocity at the free surface. The width of the thin film is considered $y = h(t)$ and T stands for the temperature.

The proposed idea of the porous and variable space is defined as[28,29]

$$\begin{aligned} K(x) &= \frac{m^2\lambda(x)^3}{(1-\lambda(x))^2},\\ \lambda(x) &= \lambda_0\left[1 + \lambda_1\exp\left(\frac{x\lambda_2}{m}\right)\right], \quad \lambda(x) \neq 1, \end{aligned} \tag{5}$$

where $h(t)$ is the film thickness, $u_{\rm w}$ is the surface velocity. While λ_1 and λ_2 are the empirical constant subject to porous particle diameter, λ_0 represents the ambient porosity. The diameter of the particle is m as shown in Refs. [28,29]. The range for the variable porous space parameters is considered $(0 < m,\ \lambda_0, \lambda_1, \lambda_2 < 1)$ that is satisfactory for the stable flow field.[28]

The dimensionless variables are as follows:[7,8]

$$\begin{aligned} &\psi(x,y,t) = (\upsilon_{\rm f} b)^{1/2}(1-\gamma t)^{-1/2} x F(\eta),\\ &u = \frac{\partial \psi}{\partial y}, \quad v = -\frac{\partial \psi}{\partial y}, \quad \eta = \left(b^{-1}\upsilon_{\rm f}(1-\gamma t)\right)^{-1/2} y,\\ &T(x,y,t) = T_0 - T_{\rm r}\left[bx^2(2\upsilon_{\rm f})^{-1}\right](1-\gamma t)^{-3/2}\theta(\eta),\\ &\beta = b\upsilon_{\rm f}^{-1}(1-\gamma t)^{-1/2} h(t). \end{aligned} \tag{6}$$

We get the following coupled system of ODEs (ordinary differential equations) by using Eq. (6) in Eqs. (1)–(5)

$$F''' + \frac{\mu_{\rm f}}{\mu_{\rm hnf}}\frac{\rho_{\rm hnf}}{\rho_{\rm f}}\left[FF'' - (F')^2 - S\left(F' + \frac{\eta}{2}\right)f''\right] - \frac{1}{Da}\left[\lambda_0^3\left(1 + \lambda_1\exp\left(\frac{-\lambda_2\eta}{\sqrt{Da}}\right)\right)\right]^{-3}\left[1 - \lambda_0\left(1 + \lambda_1\exp\left(\frac{-\lambda_2\eta}{\sqrt{Da}}\right)\right)\right]^2 F' = 0, \tag{7}$$

$$\frac{k_{\rm hnf}}{k_{\rm f}}\theta'' + Pr\frac{(\rho C_p)_{\rm hnf}}{(\rho C_p)_{\rm f}}\left[F\theta' - 2F'\theta - \frac{S}{2}(3\theta + \eta\theta')\right] + \frac{\mu_{\rm hnf}}{\mu_{\rm f}}PrE_{\rm c}(F'')^2 = 0. \tag{8}$$

After using the similarity transformation adopted from the stream function in Eq. (6), it is used in Eq. (4) to transform the physical conditions.

$$\begin{aligned} &F(0) = 0, \quad F(\beta) = \frac{S\beta}{2}, \quad F'(0) = 1,\\ &F''(\beta) = 0, \quad \theta(0) = 1, \quad \theta'(\beta) = 0. \end{aligned} \tag{9}$$

In Eq. (9), β is the thickness of the liquid film and S is the unsteadiness.

The embedded parameters that are derived after the similarity transformation are categorized as

$$\begin{aligned} S &= \frac{\gamma}{b}, \quad Pr = \frac{\mu_{\rm f} C_p}{k_{\rm f}},\\ E_c &= \frac{U_{\rm w}^2}{C_p(T_{\rm w} - T_0)}, \quad Da = \frac{\upsilon_{\rm f}}{\alpha m^2}. \end{aligned} \tag{10}$$

The embedded parameters are the unsteadiness parameter S, the Prandtl number Pr, the Eckert number $E_{\rm c}$, and the permeability parameter Da.

Thermo-physical properties of the hybrid nanofluid are formulated below:

$$\frac{\rho_{\rm hnf}}{\rho_{\rm f}} = \left(1 - \varphi_{\rm TiO_2}\right)\left[(1-\varphi_{\rm Cu}) + \varphi_{\rm Cu}\frac{\rho_{\rm Cu}}{\rho_{\rm f}}\right] + \varphi_{\rm TiO_2}\frac{\rho_{\rm TiO_2}}{\rho_{\rm f}}, \quad \frac{\mu_{\rm hnf}}{\mu_{\rm f}} = \frac{1}{\left(1-\varphi_{\rm TiO_2}\right)^{2.5}(1-\varphi_{\rm Cu})^{2.5}},$$

$$\frac{(\rho cp)_{\rm hnf}}{(\rho cp)_{\rm f}} = (1-\varphi_{\rm TiO_2})\left[(1-\varphi_{\rm Cu})+\varphi_{\rm Cu}\frac{(\rho cp)_{\rm Cu}}{(\rho cp)_{\rm f}}\right]+\varphi_{\rm TiO_2}\frac{(\rho cp)_{\rm TiO_2}}{(\rho cp)_{\rm f}},$$
$$\frac{k_{\rm hnf}}{k_{\rm nf}} = \left(\frac{k_{\rm Cu}+2k_{\rm nf}+(k_{\rm Cu}-k_{\rm nf})2\varphi_{\rm Cu}}{k_{\rm Cu}-2k_{\rm nf}+(k_{\rm Cu}-k_{\rm nf})\varphi_{\rm Cu}}\right), \quad \frac{k_{\rm nf}}{k_{\rm f}} = \left(\frac{k_{\rm TiO_2}+2k_{\rm f}-2\varphi_{\rm TiO_2}(k_{\rm f}-k_{\rm TiO_2})}{k_{\rm TiO_2}+2k_{\rm f}+\varphi_{\rm TiO_2}(k_{\rm f}-k_{\rm TiO_2})}\right). \tag{11}$$

The physical parameters of interest are displayed as

$$C_{\rm f} = \frac{2\tau_{\rm w}}{\rho U_{\rm w}^2}, \quad N_{\rm u} = \frac{q_{\rm w}x}{k(T_{\rm w}-T_0)},$$
$$\tau_{\rm w} = \mu_{\rm hnf}\left.\frac{\partial u}{\partial y}\right|_{y=0}, \quad q_{\rm w} = -k_{\rm hnf}\left.\frac{\partial T}{\partial y}\right|_{y=0}. \tag{12}$$

These equations are shear stress and heat flux. The use of the similarity variables makes the above quantities as

$$Re^{1/2}C_{\rm f} = -\frac{\mu_{\rm f}}{\mu_{\rm hnf}}F''(0), \quad Re = \frac{xU_{\rm w}}{\upsilon},$$
$$Re^{-1/2}Nu = -\frac{k_{\rm hnf}}{k_{\rm f}}\theta'(0). \tag{13}$$

The thermo-physical features of TiO_2, Cu, and H_2O are shown in the following Table 1.

Table 1. Thermo-physical features of TiO_2, Cu, and H_2O.[11]

Properties	H_2O	TiO_2	Cu
ρ (kg/m^3)	997.1	4250	8933
k (W/mK)	0.613	8.953	400
C_p (J/kg·K)	4179	686.2	385
$\beta(1/k)\times10^{-5}$	21	0.9	1.89

3. Analytical method HAM

In science and engineering, analytical methods[30–35] are mostly employed. The HAM is one of the series methods providing analytical solutions to nonlinear problems. This method is an easy tool. Just needs an initial guess to run the system and collect the series solution. The ANN method utilizes this technique to obtain a machine-based solution.

4. ANN-solution procedure

An artificial neural network (ANN) analysis is utilized to solve the problem of thin-film Cu and TiO_2 hybrid nanofluids flow on an unsteady stretching surface, taking into account that the flow medium is porous and variable.[27,36–38] The ANN worked on the already obtained solution through any analytical or numerical method. In the present work, the solution is obtained using the HAM technique. The HAM is an analytical method that provides the series solution by using the initial guess. The ANN is then applied by utilizing the HAM solution. The main steps of the ANN are as follows.

The parameters S, Da, $\varphi_{\rm Cu}$, $\varphi_{\rm TiO_2}$, Pr, $E_{\rm c}$, and β of the model problems are used initially as the data set in ANN which describes the thin film HNF flow over stretching sheet for the HT applications.

In the next step, the data collection is managed and stabilized which confirms that the input parameters S, Da, $\varphi_{\rm Cu}$, $\varphi_{\rm TiO_2}$, Pr, $E_{\rm c}$, and β are within an appropriate range for the ANN. The data collection is then forwarded neural network having several hidden layers for the proposed thin film flow problem. Furthermore, the data is divided into a set of validations and training. The set that trains from the data is used to regulate the weights and biases of the network using the iterative process. The trained ANN predicts the thin film flow of HNF and heat transfer features for the given physical conditions. The parameters S, Da, $\varphi_{\rm Cu}$, $\varphi_{\rm TiO_2}$, Pr, $E_{\rm c}$, and β are worked as the input variables and the outputs are achieved based on the provided input data.

5. Results and discussion

The solution is obtained through the HAM techniques by using the Mathematica software. The obtained results are then used for testing, and training using ANN. Figures 2(a)–2(d) show how the ANN models and Mathematica solution are shown visually. The purpose of these sketches is to illustrate how the porosity factor Da increases the velocity distribution $F'(\eta)$ and to compare the results of artificial neural networks (ANNs) and Mathematica software. As shown in Fig. 2(a), where the solution is derived using Mathematica software, a rise in the porosity factor Da for both nanofluids results in a growth in the velocity distribution $F'(\eta)$ mostly because of the extended flow networks offered by the porous medium. A larger value of (Da) means provides empty spaces inside the porous structure consequently resulting in more fluid passing through the medium.

This means that the thin film flow of HNFs over the extending surface increases. This means that increasing porosity stimulates better fluid absorptivity and flow, which raises the fluid motion of the thin film. The same analysis is promoted through (ANN) solution for the influence of Da on $F'(\eta)$ as shown in Fig. 2(b). These results show that increasing in $F'(\eta)$ is more functional way to go for an increase in Da than using Mathematica software to obtain the same parameter's influence on velocity. The effect comparison on $F'(\eta)$ with upsurge in Da between Mathematica and artificial neural net-

works (ANNs) strengthens the outcomes produced by ANNs.

The heightened sensitivity in the results may indicate that ANNs are better suited to capture complex dependencies due to their ability to adapt to non-linear interactions and learn from vast datasets. Figure 2(c) shows the investigation of absolute error in terms of the (AE) using the (ANN) models to approve the correctness requirements. The calculated absolute error values for each model fall into the specific preset ranges of 10^{-7} to 10^{-3} for the ANN setups.

As a result, the impacts of Da on $F'(\eta)$ are more accurately detected and represented by the ANN approach. This suggests that the ANNs technique is a more accurate and complete tool by consolidating the validity and reliability of the consequences acquired through it as shown from the fitting function in Fig. 2(d). The obtained results from the ANN in terms of the fitting function are used in the form of absolute error, testing, training, and validation. These outputs authenticate the degree of accuracy when compared with reference outputs.

The thickness of the thin film HNFs versus $F'(\eta)$ is shown in Figs. 3(a)–3(d) using HAM, ANN, AE, and fitting function respectively. The variation in the thickness β of the liquid film varies the viscosity of the HNFs. As the film thickness β increases, the viscosity of the fluid increases, reducing the fluid flow as shown in Figs. 3(a) and 3(b) using the HAM and ANN strategy. The capillary action is more prominent in the case of the thin film thickness during the fluid motion. Physically, the film thickness β influences the capillary forces, causing the way the hybrid nanofluid interacts with the permeable space. Intermolecular forces govern this interaction, and changes in film thickness alter these forces.

The porous medium's permeability is also an essential element and has an impact on the thin film thickness β. The porous structure's ability to flow liquid is influenced by changes in the thickness of the liquid film β. The boundary conditions imposed on the system also have an impact on the velocity profile $F'(\eta)$. So these all are the factors that control the fluid motion in case of the variation in β. The AE performance during the fluid motion varying the thickness of the HNFs is shown in Fig. 3(c). The fitting function that has a primary role in training, testing, and validation in ANN is displayed in Fig. 3(d) versus the increasing values of β. The input data and output targets validate the obtained results.

A more detailed description of the system, including variation in its porous media, fluid properties, and boundary conditions, would likely be necessary to understand the detailed relationship between the unsteadiness S and the velocity profile $F'(\eta)$ as displayed in Figs. 4(a)–4(d).

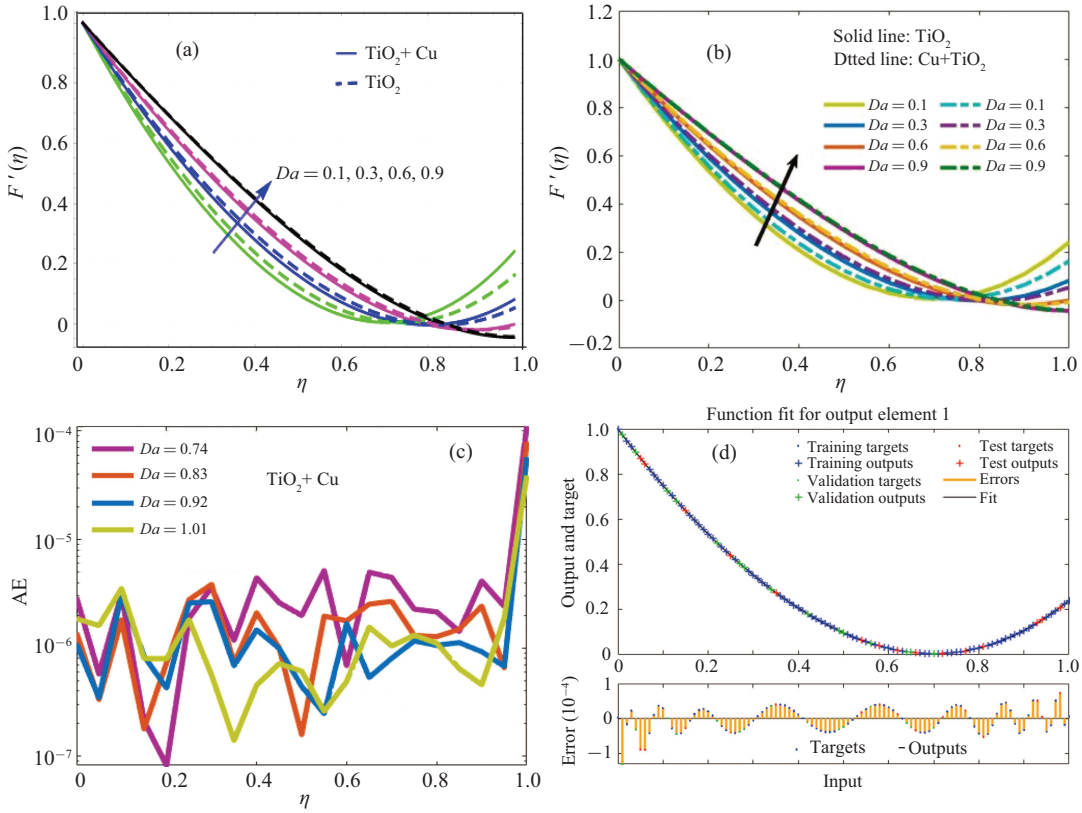


Fig. 2. The HAM outputs and ANN design for the influence of Da on $F'(\eta)$ with error estimation and fitting curve. (a) Disparities in Da versus $F'(\eta)$ for $Cu+TiO_2$ with Mathematica software, (b) disparities in Da versus $F'(\eta)$ in case of $Cu+TiO_2$ with ANN, (c) absolute error for Da in case of $Cu+TiO_2$ with ANN, (d) function fit for Da versus $F'(\eta)$ in the case of $Cu+TiO_2$ with ANN.

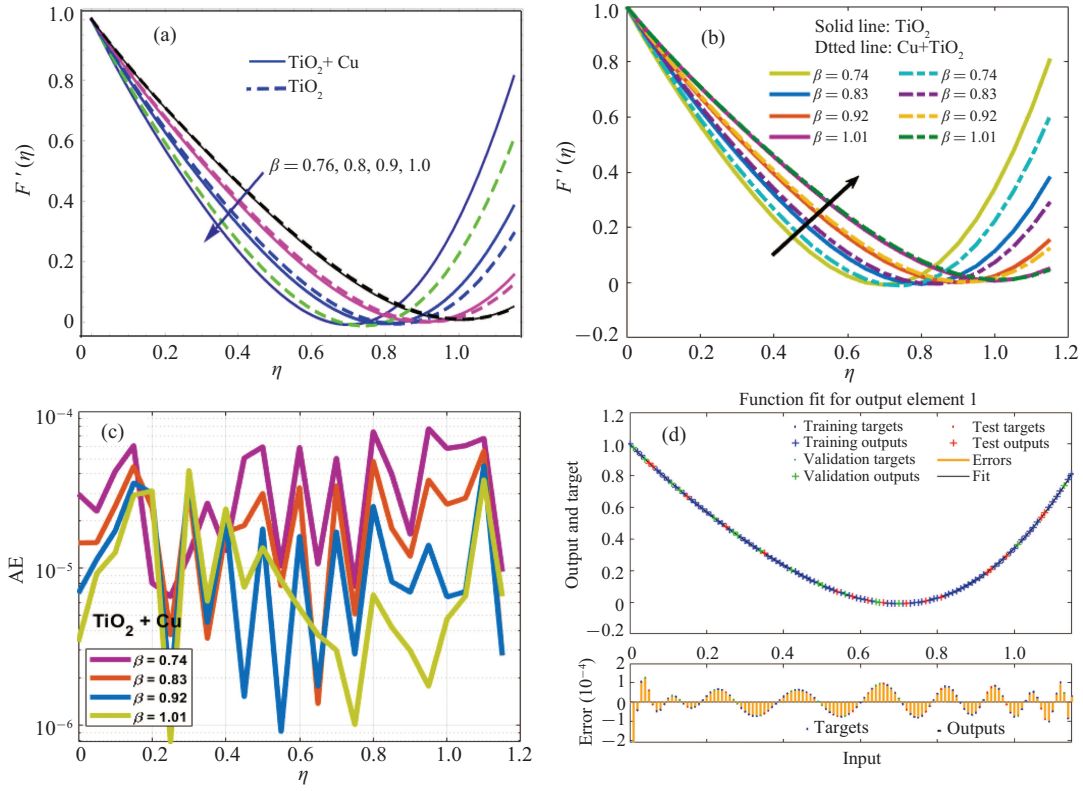


Fig. 3. (a) Disparities in β versus $F'(\eta)$ for $Cu + TiO_2$ with Mathematica software, (b) disparities in β versus $F'(\eta)$ for $Cu + TiO_2$ with ANN, (c) absolute error for β in case of $Cu + TiO_2$ with ANN, (d) function fit for β versus $F'(\eta)$ in the case of $Cu + TiO_2$ with ANN.

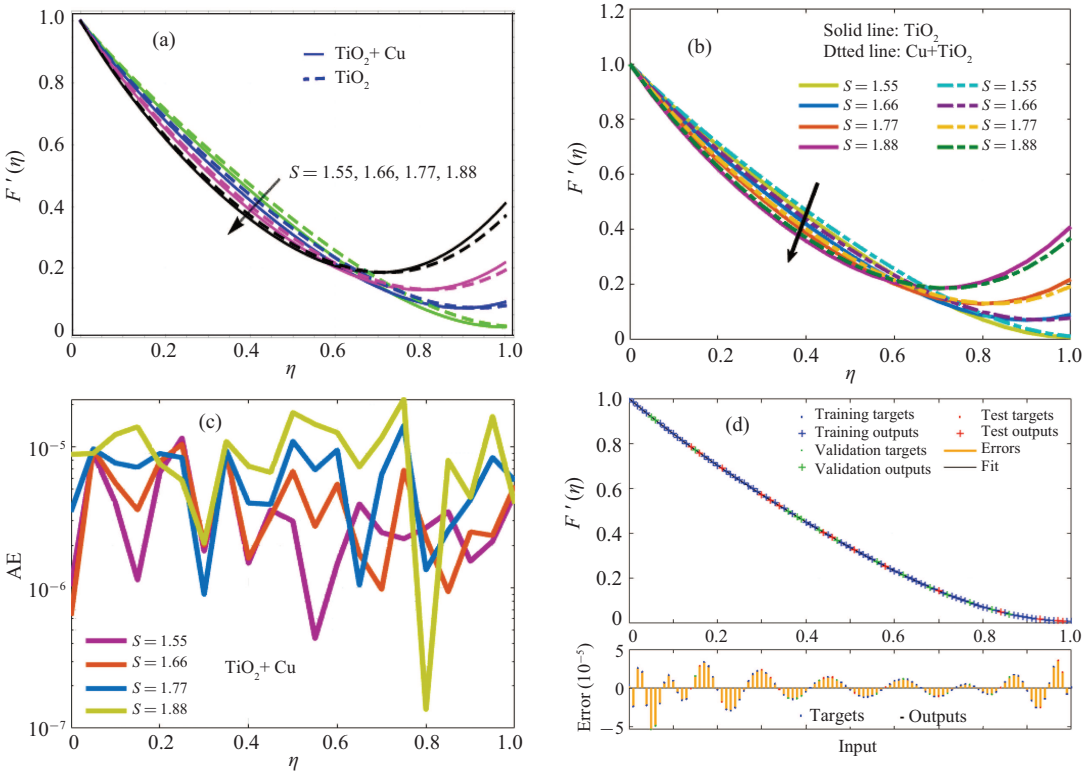


Fig. 4. (a) Disparities in S versus $F'(\eta)$ for $Cu + TiO_2$ with Mathematica software, (b) disparities in S versus $F'(\eta)$ in case of with ANN, (c) absolute error for S in case of $Cu + TiO_2$ with ANN, (d) Function fit for S in case of $Cu + TiO_2$ with ANN.

In the context of thin film liquid flow through porous media, it is possible to observe several effects as a result of the decreasing effect of an unsteadiness parameter S on the velocity field $F'(\eta)$. Variations or fluctuations in flow conditions over time are typically associated with unsteadiness parameters S. A more stable and steady-state flow may be possible with a decrease in the unsteadiness parameter.

The velocity field $F'(\eta)$ has the potential to become more

uniform and predictable over time as the variations in flow conditions decrease and depend on S. The pulsaturity of the flow is often associated with an unsteadiness parameter. The pulsations or oscillations in the velocity field $F'(\eta)$ will probably decrease when the unsteadiness parameter S decreases. The impact is visible in Figs. 4(a) and 4(b) using HAM and ANN procedures. This S has the potential to produce a flow that is smoother and more consistent. The attenuation of waves can occur when the unsteadiness parameter S decreases in systems with wave-like behavior, like peristaltic flows. As the system approaches a more steady-state condition, there may be a decline in both amplitude and frequency of waves in the velocity field $F'(\eta)$. Where the AE performance is displayed in Fig. 4(c). Variations in velocity magnitude and direction are caused by transient effects caused by unsteadiness in the flow. Less pronounced transient effects will result in a more stable velocity field as the unsteadiness parameter decreases. As the unsettledness decreases, the interaction between liquid and porous media may become simpler. The fitting curve to valdate the obtained results through training, testing is displayed in Fig. 4(d).

Figures 5(a)–5(d) as the thickness β of the liquid film decreases, the heat conduction across the film becomes more efficient. A faster exchange of thermal energy is achieved through thinner films due to their shorter path for heat to travel from the hot to the cold side. As the thickness decreases, convection flows more capably transfer heat away from the surface, paying to an operative cooling to the system. Thicker films enhance the resistance to thermal factors, reducing the heat transfer rate. The thinner behavior of the β condense this thermal resistance, permitting a speedy exchange of thermal energy between the hybrid nanofluids and porous space as shown in Figs. 5(a) and 5(b) using HAM and ANN approaches. The AE performance using the variation in β versus the temperature profile utilizing the ANN is shown in Fig. 5(c). The smaller error detection approves the obtained results. The fitting function is an important part of the ANN strategy to validate the results using the testing and training to validate the thin film β variation versus the temperature distribution as shown in Fig. 5(d).

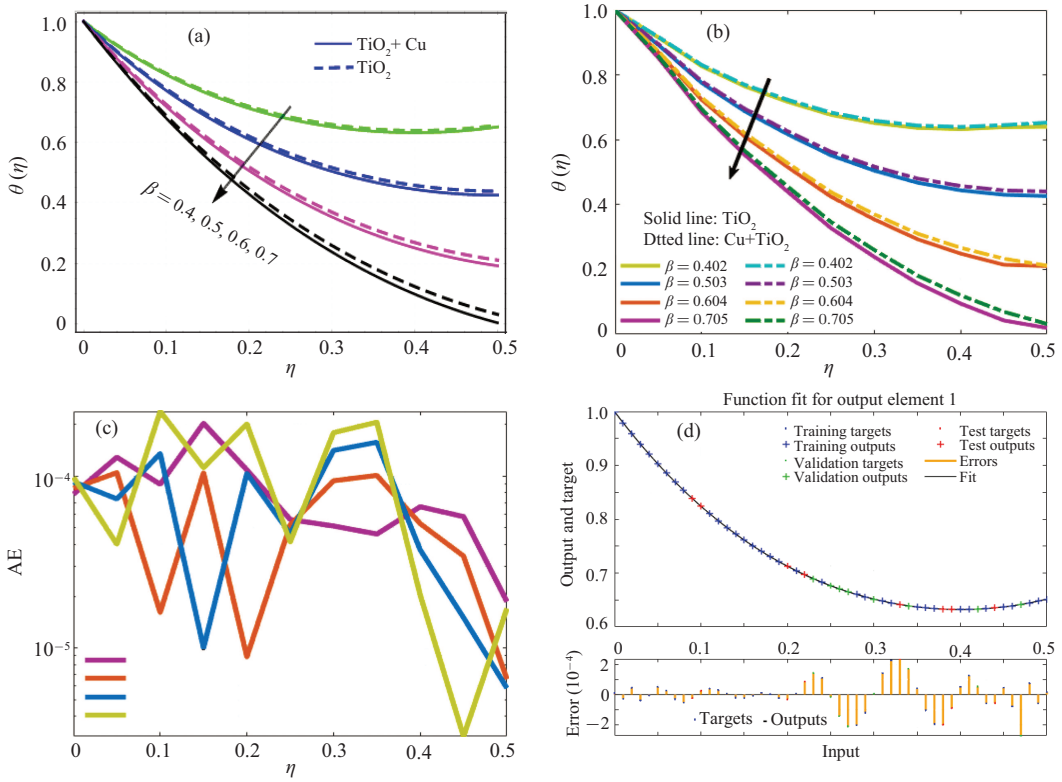


Fig. 5. (a) Disparities in β versus $\theta(\eta)$ for $Cu + TiO_2$ with Mathematica software, (b) disparities in β versus $\theta(\eta)$ in case of $Cu + TiO_2$ with ANN, (c) absolute error for β in the case of $Cu + TiO_2$ with ANN, (d) function fit for β in the case of $Cu + TiO_2$ with ANN.

The impact of the unsteadiness term S versus the temperature profile is displayed in Figs. 6(a)–6(d). The increasing effect of an unsteadiness parameter S on the temperature profile in the context of thin film liquid flow through porous media has an important role to improve the HT rate displayed in Figs. 6(a) and 6(b) using the HAM and ANN techniques. The larger values of S reducing the flow of the thin film HNFs and consequently improve the thermal performance of the $Cu + TiO_2$ HNFs. This impact is quite more extensive near the sheet surface when the thickness of the liquid film is thin. As

the S rises, the perturbations in the flow are likely to become more substantial affecting the velocity distribution in the thin liquid film. In fact, increasing unsteadiness indicates a larger impact of transient effects in the thin film HNF flow. Since the thin film flow of HNF is considered, a variable porous space becomes more complex with increasing unsteadiness S and the slowness of the liquid film provide more heating. The AE representation of S in case of the temperature distribution is shown in Fig. 6(c). Where the validation of the unsteadiness parameter through fitting function is displayed in Fig. 6(d).

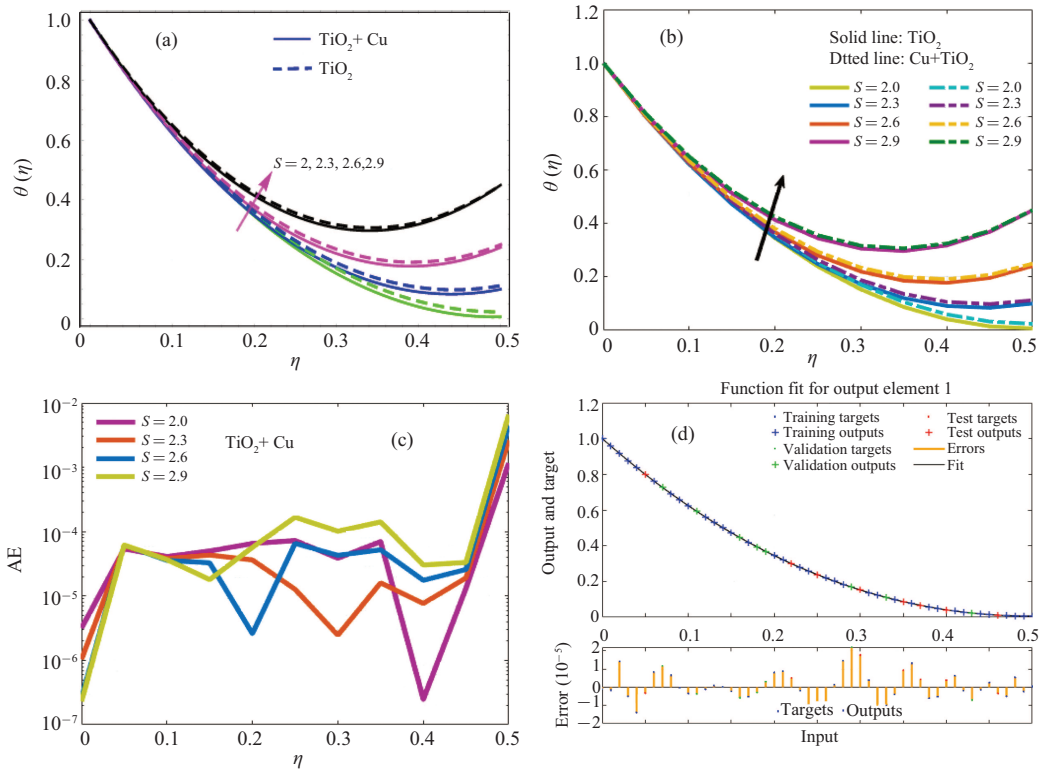


Fig. 6. (a) Disparities in S versus $\theta(\eta)$ for $Cu + TiO_2$ with Mathematica software, (b) disparities in S versus $\theta(\eta)$ in the case of $Cu + TiO_2$ with ANN, (c) absolute error for S in case of $Cu + TiO_2$ with ANN, (d) function fit for S versus $\theta(\eta)$ in the case of $Cu + TiO_2$ with ANN.

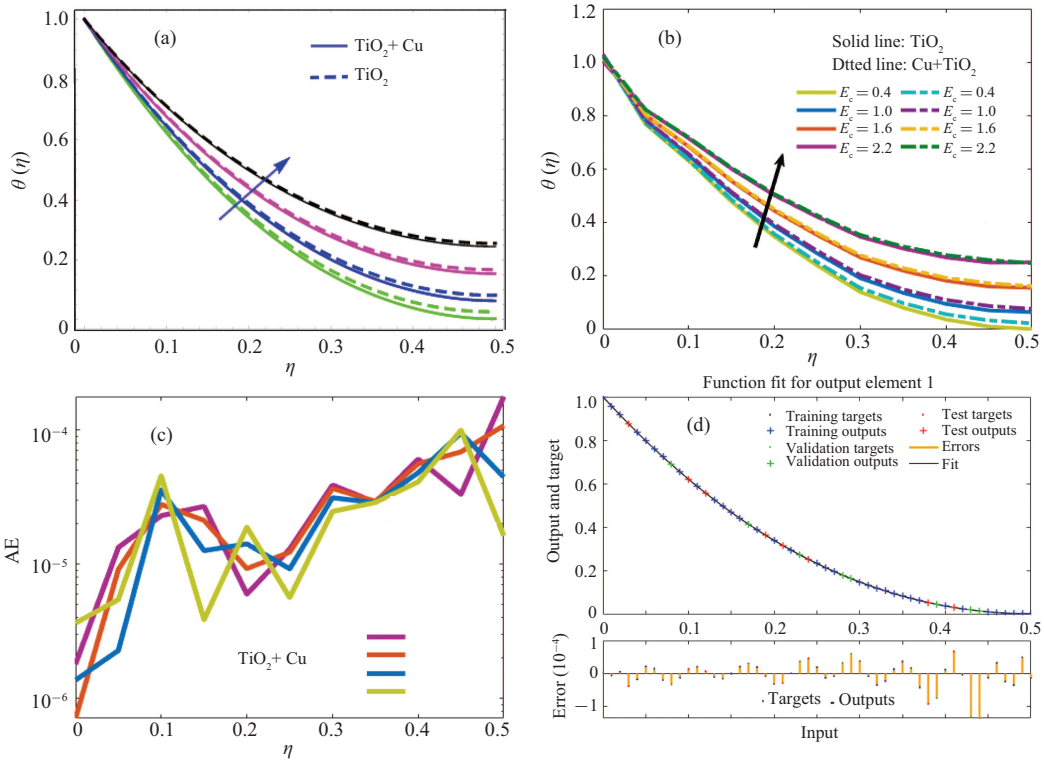


Fig. 7. (a) Disparities in E_c versus $\theta'(\eta)$ for $Cu + TiO_2$ with Mathematica software, (b) disparities in E_c versus $\theta'(\eta)$ in the case of $Cu + TiO_2$ with ANN, (c) absolute error for E_c in case of $Cu + TiO_2$ with ANN, (d) function fit for E_c versus $\theta'(\eta)$ in the case of $Cu + TiO_2$ with ANN.

Figures 7(a)–7(d) illustrate the influence of Eckert number E_c on temperature distribution $\theta(\eta)$ with respect to Mathematica solution Fig. 7(a) and ANNs solution Fig. 7(b), while figure 7(c) illustrates the absolute error analysis. Similarly the fitting function to validate the obtained results is shown in Fig. 7(d). Figures 7(a) and 7(b) illustrate that as E_c increases, the appropriate extension of the thermal distribution happens. In fact,, E_c is a dimensionless number that, in the context of convective heat transfer, defines the ratio of kinetic energy to enthalpy. $\theta(\eta)$ may be significantly compressed by a rise in the E_c. E_c increase means that the fluid's kinetic energy is more than the thermal energy involved. In these situations, a rise in E_c denotes a rise in the flow's kinetic energy. This increased kinetic energy implies that there is more energy in the fluid that may be used to dissipate heat.

Table 2 shows the increment in skin friction occurrence when the values of different parameters become increase.

Table 2. The increment in skin friction occurrence when the values of different parameters increase.

Da	$\varphi_1+\varphi_2$	S	$\mu_{nf}\mu_f F''(0)$ Cu	$(\mu_{hnf}/\mu_f)F''(0)$ Cu + TiO_2
0.1	0.01	0.1	**0.53278194**	**0.54287196**
0.2			0.542672198	0.55218979
0.3			0.552781902	0.56319082752
0.1	**0.01**	**0.1**	**0.53278194**	**0.54287196**
	0.02		0.54278187	0.552781961
	0.03		0.54982109	0.563675210
0.1	**0.01**	**0.1**	**0.53278194**	**0.54287196**
		0.3	0.53672891	0.548290871
		0.5	0.54190823	0.551962521

In Table 3, we listed the Nusselt number $Re_r^{1/2}Nu_r = -k_{hnf}/k_f\theta'(0)$ versus various factors.[7,8]

Table 3. Nusselt number versus various factors.

$\varphi_1+\varphi_2$	S	E_c	$-k_{nf}/k_f\theta'(0)$ Cu	$-k_{hnf}/k_f\theta'(0)$ Cu + TiO_2
0.0	**1**	**1**	**3.13257819**	**3.276743210**
0.01			3.183245167	3.3416543765
0.02			3.219866232	3.41654843
0.03			3.2782761	3.463786
0.04			3.317821	3.536543276
0.05			3.35367219	3.58432171
0.0	**1**	**1**	**3.13257819**	**3.276743210**
	3		3.10652718	3.2597190
	5		3.01872891	3.23167287
0.0	**1**	**1**	**3.13257819**	**3.276743210**
		3	3.1563219	3.256527891
		5	3.164251	3.26763972

The AE performance to obtain the error estimation has been shown in Fig. 7(c). The validation of the increasing values of E_c versus thermal profile using the testing, training has been shown in Fig. 7(d). The fitting function used in this scenario validating the obtained results by means of the ANN procedure.

The thermophysical properties are displayed in Table 1. The skin friction versus physical parameters displayed in Table 2. The heat transfer (HT) rate using various embedded parameters has been shown in Table 3. The increasing values of $\varphi_1+\varphi_2$, S, Da improving the skin friction. In fact, the resistive force increasing with the larger amount of these parameters. The HT rates improves with Eckert number E_c and NPs volume fraction $\varphi_1+\varphi_2$.

Table 4 shows the percentage variation in Nusselt number with growth in nanoparticles by using the following relation.

$$\text{Increase} = \frac{\text{With nanoparticles}}{\text{Without nanoparticles}} \times 100 = \text{Result},\ \text{Result} - 100 = \%\,\text{enhancment}.$$

Table 4. Percentage variation in Nusselt number with growth in nanoparticles by using the above relation.

φ_1 and φ_2	$-k_{nf}/k_f\theta'(0)$ Cu-nanofluid	$-k_{hnf}/k_f\theta'(0)$ Cu + TiO_2-hybrid nanofluid
0.00	0% increase	0% increase
0.01	1.617% increase	1.980% increase
0.02	2.78% increase	4.26% increase
0.03	4.65% increase	5.59% increase
0.04	5.91% increase	7.728% increase
0.05	7.05% increase	9.38% increase

The increasing nanoparticle volume fraction implies enhanced HT properties, as NPs have higher thermal conductivity compared to traditional fluids. This characteristic allows for efficient heat dissipation and enhanced thermal management in various systems. On the other hand the increasing values of S decline the HT rate. The percentage-wise enhancement in HT rate versus is shown in Table 4. The HT rate improves up to 7.05% using nanofluid, while the HT rate enhances up to 9.38% using HNFs volume fraction $\varphi_1+\varphi_2$ 0.01 to 0.05.

Table 5 presents the numerical values for various features in the ANN models. The performance based on testing, train-

ing, and validation are displayed using the values for MSE. ANN models have become an excellent choice for modeling and calculating various phenomena, including the flow of thin film HNFs. The significance of various structures in these ANN models is described in Table 5. The performance of an ANN model in terms of precision and efficiency is critical. The estimations of the behavior of thin film HNFs flow are observed for their good agreement. A good agreement is perceived which confirms reliable estimates and diminishes errors in the form of numerical simulations as shown in Table 5. Testing of ANN models is important to assess their simplification fitness. The tested model precisely predicted the thin film HNF flow behavior for data that it had not met in the training phase. Testing helps identify the model's limitations and possible areas for perfection as shown in Table 5. The training algorithm and convergence principles meaningfully determined the precision of the model as accomplished for the present model in Table 5. Validation involves measuring the presentation and accuracy of the ANN model using autonomous datasets in the form of parameters. Validation guarantees that the model is reliable to make precise predictions for hidden data, making it a vital aspect of building consistent ANN models for thin film HNFs flow.

Table 5. Numerical outputs of the ANN.

Cases	MSE			Performance	Gradient	Mu	Epoch	Time (s)
	Training	Validation	Testing					
1	1.2571×10^{-8}	8.32×10^{-7}	2.11×10^{-7}	7.23×10^{-8}	1.39×10^{-5}	1.00×10^{-6}	820	02
2	2.31×10^{-8}	3.53×10^{-8}	3.87×10^{-8}	4.35×10^{-8}	8.65×10^{-6}	1.00×10^{-6}	682	02
3	4.23×10^{-7}	6.52×10^{-7}	1.82×10^{-7}	2.89×10^{-7}	3.21×10^{-6}	1.00×10^{-6}	512	01
4	3.21×10^{-9}	5.42×10^{-9}	2.83×10^{-9}	1.87×10^{-9}	8.63×10^{-6}	1.00×10^{-7}	892	04
5	3.24×10^{-8}	3.01×10^{-8}	1.35×10^{-7}	2.62×10^{-8}	1.42×10^{-4}	1.00×10^{-7}	1000	04

6. Conclusion

The thin film of Cu and TiO_2 hybrid nanofluid over an unsteady extending surface in a variable porous space is considered for the optimization of heat transfer. The transform problem is solved using the HAM technique. The HAM results are then handled by ANN technique to validate the obtained results by testing, training, AE, and fitting function.

The ANN technique allows for a more precise illustration to handle the complex flow models, which are not possible through traditional methods. In conclusion, the artificial neural network (ANN) analysis verifies an operative tool in solving the problem of thin-film Cu and TiO_2 hybrid nanofluids flow on an unsteady stretching surface, in view of the porous and variable nature of the flow medium. The main outputs are listed below.

(i) The increased values the φ_{Cu}, φ_{TiO_2}, Da, β result in a decrease in HNF motion, indicating increased resistance to flow. This is beneficial in terms of energy consumption and whole system efficiency.

(ii) The HNFs flow containing Cu and TiO_2 nanoparticles has shown a significant increase in the liquid film thickness β compared to the base fluid. This suggests that the addition of these nanoparticles has a positive impact on enhancing the flow characteristics and increasing the liquid film thickness β.

(iii) The use of thin film Cu and TiO_2 hybrid nanofluid flow establishes a promising trend of increasing values of the φ_{Cu}, φ_{TiO_2}. The increasing nanoparticle volume fraction φ_{Cu}, φ_{TiO_2} implies enhanced HT properties, as nanoparticles have higher thermal conductivity compared to traditional fluids. This characteristic allows for efficient heat dissipation and improved thermal management in various systems.

(iv) The percentage-wise heat transfer is calculated using the Cu-nanofluid and $Cu + TiO_2$-hybrid nanofluid. It is observed that up to the maximum quantity of φ_{Cu}, φ_{TiO_2} increasing the HT rate 7.05% and 9.38% respectively.

(v) ANN model for thin film HNFs flow over an unsteady stretched surface ensures precise predictions, reliable generalization, adaptive learning, and continuing validation.

Table 6 displays the common parameters that are taken into account to compare the present work with the existing literature. A very closed agreement has been observed that validates the present analysis.

Table 6. The common parameters taken into consideration by comparing the present analysis with the published work.

Common parameters		Qasim *et al.*[39]	Nasir *et al.*[40]	Present work
S	β	$F''(0)$	$F''(0)$	$F''(0)$
0.2	0.50	0.1642783942	0.1644527839	0.1644462712
0.4		0.1742783901	0.1743426567	0.1743536728
0.6		0.1842563190	0.1844267523	0.1844324626
0.8		0.1942786513	0.1945234127	0.1945324152
	0.55	0.1824516726	0.1824256374	0.1824324782
	0.60	0.2034256178	0.2035327814	0.2035452781
	0.65	0.2252642718	0.2253257212	0.2253325625

The current project is centered around variable porous media. The future work can be extended to incorporate the variable Darcy–Forchheimer thin film concept. Different

nanoparticles can be added with the addition of magnetic and electric fields as well. The Riga Plate concept is also useful to consider this film flow in various fields of science and engineering. The entropy regime is a valuable addition to this study as a future work.

References

[1] Neeraas B O, Fredheim A O and Aunan B 2004 *Int. J. Heat Mass Transfer* **47** 3565

[2] Weinstein S J and Ruschak K J 2004 *Annu. Rev. Fluid Mech.* **36** 29

[3] Ibrahim H T, Qiang H, Al-Rekabi W S and Qiqi Y 2012 *Pakistan Journal of Nutrition* **11** 610

[4] Nicolella C, Van Loosdrecht M C M and Heijnen J J 2000 *Journal of biotechnology* **80** 33

[5] Vo T Q, Park B, Park C and Kim B 2015 *J. Mech. Sci. Technol.* **29** 1681

[6] Craster R V and Matar O K 2009 *Rev. Mod. Phys.* **81** 1131

[7] Khan N S, Islam S, Gul T, Khan I, Khan W and Ali L 2018 *Alexandria Engineering Journal* **57** 1019

[8] Ali L, Islam S, Gul T, Khan I, Dennis C C, Khan W and Khan A 2017 *Appl. Sci.* **7** 404

[9] Mebarek-Oudina F, Preeti Sabu A S, Vaidya H, Lewis R W, Areekara S and Ismail A I 2024 *Int. J. Mod. Phys. B* **38** 2450003

[10] Ali A, Mebarek-Oudina F, Barman A, Das S and Ismail A I 2023 *Journal of Thermal Analysis and Calorimetry* **148** 7059

[11] Ahmad S, Ali K, Faridi A A and Ashraf M 2021 *Int. Commun. Heat Mass Transfer* **129** 105708

[12] Jana S, Salehi-Khojin A and Zhong W H 2007 *Thermochimica Acta* **462** 45

[13] Mannu R, Karthikeyan V, Velu N, Arumugam C, Roy V A, Gopalan A I and Kannan V 2021 *Nanomaterials* **11** 440

[14] Shahzadi I and Bilal S 2020 *Computer Methods and Programs in Biomedicine* **187** 105248

[15] Ketchate C G N, Kapen P T, Fokwa D and Tchuen G 2021 *Informatics in Medicine Unlocked* **27** 100800

[16] Xiong Q, Altnji S, Tayebi T, Izadi M, Hajjar A, Sundén B and Li L K 2021 *Sustainable Energy Technologies and Assessments* **47** 101341

[17] Khodadadi H, Aghakhani S, Majd H, Kalbasi R, Wongwises S and Afrand M 2018 *Int. J. Heat Mass Transfer* **127** 997

[18] Waseem M, Gul T, Khan I, Khan A, Saeed A, Ali I and Kumam P 2021 *Sci. Rep.* **11** 17498

[19] Ramzan M, Riasat S, Aljurbua S F, Ghazwani H A S and Mahmoud O 2022 *Nanomaterials* **12** 1794

[20] Sun X, Zhang Y, Chen G, Liu T, Ren D, Ma J and Karwani S 2018 *Energy & Fuels* **32** 11118

[21] Xian H W, Sidik N A C and Saidur R 2020 *Int. Commun. Heat Mass Transfer* **110** 104389

[22] Mukhopadhyay S, De P R, Bhattacharyya K and Layek G C 2013 *Ain Shams Engineering Journal* **4** 933

[23] Andersson H I, Aarseth J B and Dandapat B S 2000 *Int. J. Heat Mass Transfer* **43** 69

[24] Park S, Atwair M, Kim K, Lee U, Na J, Zahid U and Lee C J 2021 *Journal of Industrial and Engineering Chemistry* **98** 327

[25] Martorell J, Santomá P, Molins J J, García-Granada A A, Bea J A, Edelman E R and Balcells M 2012 *Ann. New York Acad. Sci.* **1254** 51

[26] Mashaghi S, Abbaspourrad A, Weitz D A and Van Oijen A M 2016 *TrAC Trends in Analytical Chemistry* **82** 118

[27] Alabdan R, Khan S U, Al-Qawasmi A R, Vakkar A and Tlili I 2021 *Case Studies in Thermal Engineering* **28** 101412

[28] Vishnuprasad S, Haribabu K and Perarasu V T 2019 *Heat and Mass Transfer* **55** 2221

[29] Alotaibi A, Gul T, Saleh Alotaibi I M, Alghuried A, Alshomrani A S and Alghuson M 2024 *Engineering Applications of Computational Fluid Mechanics* **18** 2343418

[30] Turkyilmazoglu M 2019 *Computer Modeling in Engineering & Sciences* **120** 63

[31] Alnahdi A S and Gul T 2024 *Mod. Phys. Lett. B* **38** 2450046

[32] Muhammad K, Hayat T and Momani S 2024 *Mod. Phys. Lett. B* **38** 2450160

[33] Alnahdi A S and Gul T 2024 *Chin. Phys. B* **33** 104701

[34] Nasir S, Sirisubtawee S, Juntharee P and Gul T 2024 *Chin. Phys. B* **33** 050204

[35] Khan A, Ali I, Almusawa M Y, Gul T and Alghamdi W 2023 *Chin. Phys. B* **32** 084401

[36] Alharbi S O 2024 *Journal of Thermal Analysis and Calorimetry* **149** 8289

[37] Awwad F A, Ismail E A and Gul T 2023 *Symmetry* **15** 1288

[38] Ali I, Gul T and Khan A 2023 *Mathematics* **11** 1893

[39] Qasim M, Khan Z H, Lopez R J and Khan W A 2016 *Eur. Phys. J. Plus* **131** 16

[40] Nasir S, Shah Z, Islam S, Bonyah E and Gul T 2019 *AIP Adv.* **9** 015223